

RESEARCH

Open Access



# Localization based on standard wireless LAN infrastructure using MIMO-OFDM channel state information

Tanee Demeechai<sup>1\*</sup>, Pratana Kukieattikool<sup>1</sup>, Thang Ngo<sup>2</sup> and Tae Gyu Chang<sup>2</sup>

## Abstract

An indoor localization method using multiple input, multiple output orthogonal frequency division multiplexing (MIMO-OFDM) channel state information (CSI) is proposed as a method that can be implemented on wireless local area networks of a current standard without affecting their protocol structures and that does not require a training process for adaptation to indoor environments. In the proposed method, the CSI obtained by the MIMO-OFDM receivers of all access points upon successful reception of a data packet from a mobile terminal (MT) is processed in order to determine the location of the MT. The proposed method analyzes the multipath effect that appears in the CSI as multiple complex sinusoids by using the matrix pencil method in order to extract only terms that are contributed by direct paths from the MT to the access points. Localization is achieved using the direct-path terms on the basis of the maximum likelihood principle.

**Keywords:** Indoor localization, MIMO-OFDM, Channel state information, Multipath propagation, Matrix pencil method, Maximum likelihood principle

## 1 Introduction

Indoor localization is a hot research topic in the field of wireless communication owing to its capability to provide a wide range of location-based services for increasingly ubiquitous smart mobile devices. For indoor environments, wireless local area network (WLAN) technology based on the IEEE 802.11 standards is widely employed around the world for providing data connections to mobile devices. Therefore, this paper focuses on indoor localization methods based on WLAN technology. Specifically, the purpose of this paper is to propose a localization method that can be implemented using the infrastructure of a WLAN without affecting its protocol structure. The proposed method will simultaneously exploit and be constrained by WLAN characteristics whereby WLANs are trending toward asynchronous networks of multiple input, multiple output orthogonal frequency division multiplexing (MIMO-OFDM) access points (APs) [1].

Although many studies have investigated localization [2–6], it is not straightforward to apply their results to the problem of interest without requiring dedicated infrastructure or affecting the WLAN protocol structure. A few localization methods based on the IEEE 802.11 standards have been proposed in the literature [7–9] and implemented commercially. However, most of these methods use the received signal strength indicator (RSSI) as data for location determination [7, 8]. The use of the RSSI usually requires a disincentive process of measurement-based training for adaptation to ever-changing environments because the RSSI is very sensitive to both large-scale shadowing and small-scale multipath fading prevalent in indoor environments. Recently, a method that uses channel state information (CSI) available through a network interface card [10] has been proposed [9]. Compared to the RSSI, the CSI is less sensitive to multipath fading. Nevertheless, the method proposed in [9], which is based on single-antenna APs, requires a disincentive measurement-based training process. The method proposed in the present paper uses the CSI obtained by the MIMO-OFDM receiver of each AP as data for location determination, without any measurement-based training

\*Correspondence: [tanee.demeechai@nectec.or.th](mailto:tanee.demeechai@nectec.or.th)

<sup>1</sup>National Electronics and Computer Technology Center (NECTEC), National Science and Technology Development Agency (NSTDA), 112 Thailand Science Park, Phahonyothin Road, Pathum Thani 12120, Thailand  
Full list of author information is available at the end of the article

process for adaptation to ever-changing environments. The details of the proposed method are described in subsequent sections.

## 2 Proposed localization method

According to the proposed method, the CSI obtained by the MIMO-OFDM receivers of all APs upon successful reception of a data packet from a mobile terminal (MT) is processed in order to determine the location of the MT. We assume that the MT uses only one antenna, i.e., one spatial stream, for transmitting the data packet for localization. Therefore, the packet's preamble part for estimating the CSI by the OFDM receiver of each AP will consist of only one VHT-LTF (see [1], Fig. 22–4). It may be noted that, while the standard [1] defines four OFDM signal models, classified according to the bandwidth as the 20-, 40-, 80-, and 160-MHz models, the duration of the VHT-LTF symbol equals 4  $\mu$ s including the 800-ns guard interval for all the models.

The localization method involves removing multipath reflection components in the CSI and searching for the best location on the basis of a likelihood metric. Because removing multipath reflection components in the CSI is an important step, the characteristics of indoor multipath propagation and the CSI are discussed first; then, the algorithm of the proposed method is described in detail.

### 2.1 CSI from MIMO-OFDM receivers as location information

The CSI is always required for data demodulation in an OFDM receiver. Therefore, a receiver can provide the CSI at no overhead [10]. The CSI is represented by the channel frequency response (CFR) for the set of used OFDM subcarriers. As radio wave propagation in indoor environments is subjected to multipath characteristics, we may characterize the CFR as follows. Assuming that the antennas of an AP are closely located, the CFR estimated by the receiver of the  $q$ -th AP for the  $m$ -th antenna and  $k$ -th subcarrier can be expressed by

$$H_{k,m,q} = \sum_{n=0}^{N_p-1} h_{n,q} e^{-j2\pi(f_0+kB/N)(t_q+t_{n,m,q})} + w_{k,m,q}, \quad (1)$$

where  $N_p$  is the number of paths in the channel model,  $h_{n,q}$  is the complex amplitude of the  $n$ -th path for the  $q$ -th AP,  $f_0$  is the carrier frequency,  $t_{n,m,q}$  is the propagation delay associated with the  $n$ -th path between the MT antenna and the  $m$ -th antenna of the  $q$ -th AP,  $B$  is the OFDM signal bandwidth,  $B/N$  is the OFDM subcarrier spacing,  $t_q$  is the time shift introduced by the OFDM time synchronizer of the receiver, and  $w_{k,m,q}$  is the estimation error that is assumed to behave as additive white Gaussian noise (AWGN). Note that a perfect OFDM time synchronizer

only needs to force the time shift  $t_q$  to be well within a tolerance supported by the OFDM guard interval [11]. In other words, with a guard interval length of  $t_g$ , the time shift is required to ensure that the effective delay of the shortest path is non-negative ( $t_q + \min_{n,m}(t_{n,m,q}) \geq 0$ ) while the effective delay of the longest path does not exceed the guard interval length ( $t_q + \max_{n,m}(t_{n,m,q}) \leq t_g$ ). Therefore,

$$0 \leq t_q + t_{n,m,q} \leq t_g, \forall (n, m). \quad (2)$$

This uncertainty of  $t_q$  is another source of variation of the CSI, which must be properly treated when the CSI is used for localization.

In this study, the AP antennas are closely located as an array with spacing between elements of the order of half wavelength. Therefore, the differences between the propagation times to the AP antennas for the same path manifest themselves as approximately frequency flat phase difference terms, i.e., (1) can be approximately expressed by

$$H_{k,m,q} = \sum_{n=0}^{N_p-1} h_{n,q} e^{-j(2\pi(f_0+kB/N)t_{n,q}+\phi_{n,m,q})} + w_{k,m,q}, \quad (3)$$

where  $t_{n,q} = t_q + (\sum_{\forall m} t_{n,m,q})/M_q$  with  $M_q$  is the number of antennas in the antenna array for the  $q$ -th AP, and  $\phi_{n,m,q} = 2\pi f_0(t_q + t_{n,m,q} - t_{n,q})$ . Note that the phase terms  $\phi_{n,m,q}$ ,  $1 \leq m \leq M_q$ , obey

$$\sum_{\forall m} \phi_{n,m,q} = 0 \quad (4)$$

and share a relationship that depends on the antenna array geometry for the  $q$ -th AP and the angle of arrival (AOA) to the array from the  $n$ -th path. In what follows, we shall assume that the terms in (3) have been sorted according to time delays such that  $t_{n_1,q} \leq t_{n_2,q}$  if  $n_1 \leq n_2$ . Further, it may be noted that (2) becomes

$$0 \leq t_{n,q} \leq t_g, \forall n. \quad (5)$$

We may then rearrange (3) as

$$H_{k,m,q} = \sum_{n=0}^{N_p-1} g_{n,q} e^{-j(2\pi B t_{n,q} k/N + \phi_{n,m,q})} + w_{k,m,q}, \quad (6)$$

where  $g_{n,q} = h_{n,q} e^{-j2\pi f_0 t_{n,q}}$ . We may note from (6) that for an AP antenna, the estimated CFR as a function of  $k$  is the sum of multiple sinusoids plus noise. In addition, it is the relationship between  $\phi_{0,m,q}$ ,  $1 \leq m \leq M_q$ , characterizing the sinusoids of the shortest paths to the array elements, that will contain the location information of the MT, if the shortest paths are the direct paths.

## 2.2 Proposed algorithm

The proposed algorithm consists of two major steps. The first step is to obtain CFRs that are effective for localization by minimizing irrelevant contributions from multipath reflection and the uncertainty of the OFDM time synchronizer. The second step is to search for the best location on the basis of a likelihood metric.

### 2.2.1 Obtaining an effective CFR

To minimize irrelevant contributions from multipath reflection and the uncertainty of the OFDM time synchronizer in the CFR for the  $m$ -th antenna of the  $q$ -th AP, we aim to obtain an effective CFR modeled by

$$G_{m,q} = g_{0,q} e^{-j\phi_{0,m,q}} + w_{m,q}, \quad (7)$$

where  $w_{m,q}$  denotes the average of  $w_{k,m,q}$  across  $k$ . Note that the effective CFR consists of the contribution from the shortest path and additive noise. Therefore, the effective CFR will carry information of the MT location if the shortest path is actually the direct path. Hence, the main assumption of the proposed algorithm is that direct paths between the MT and the APs exist with considerable amplitudes compared to the amplitude of the additive noise.

In the proposed algorithm, the effective CFRs for an AP are obtained by first obtaining reflection-rich CFRs for contiguous subcarriers from the CSI, then obtaining parameters of the sinusoids in the reflection-rich CFRs, and finally transforming the reflection-rich CFRs to obtain the result.

**Obtaining a reflection-rich CFR for contiguous subcarriers** According to the underlying standards [1], a CFR can be obtained from the CSI only for used OFDM subcarriers that are discontinuous. The proposed algorithm obtains the CFR for contiguous subcarriers by simply using linear interpolation to compute the CFR for unused subcarriers whenever they are between two used subcarriers. The linear interpolation method is clearly simple, but we consider whether it can effectively preserve the slow-oscillation characteristics of the shortest-path sinusoid. Hence, according to the standard signal models [1], the resulting CFR is contiguous for  $-K \leq k \leq K$ , where the values of  $K$  for the 20-, 40-, 80-, and 160-MHz signal models are 28, 58, 122, and 250, respectively.

**Obtaining parameters of sinusoids** A sinusoid as a function of  $k$ , expressed by  $ae^{j\omega k}$ , is characterized by its frequency  $\omega$  and its complex amplitude  $a$ . To estimate the frequencies of all the sinusoids in the CFRs of the  $q$ -th AP, we adopt the matrix pencil method (MPM) [12, 13] because this constant amplitude multiple-sinusoid estimation problem is equivalent to the direction-of-arrival estimation problem with fully coherent sources, which

is directly addressed by the MPM. Moreover, the MPM method has been shown to be the most suitable method among various super-resolution methods [13].

Following [13] with our own notations, we may detail the estimation procedure as follows. According to [13], a snapshot of data is a sequence of limited samples of the observation. Therefore, from the CFR data of the  $q$ -th AP, we have  $M_q$  snapshots of data, with each snapshot containing  $2K+1$  samples. Accordingly, the input data matrix is formed as

$$\mathbf{Y} = [\mathbf{Y}_1 \ \mathbf{Y}_2 \ \cdots \ \mathbf{Y}_{M_q}], \quad (8)$$

where  $\mathbf{Y}_m$  denotes the Hankel matrix for the  $m$ -th snapshot. Thus,

$$\mathbf{Y}_m = \begin{bmatrix} H_{-K,m,q} & H_{-K+1,m,q} & \cdots & H_{-K+L-1,m,q} \\ H_{-K+1,m,q} & H_{-K+2,m,q} & \cdots & H_{-K+L,m,q} \\ \vdots & \vdots & \ddots & \vdots \\ H_{K-L+1,m,q} & H_{K-L+2,m,q} & \cdots & H_{K,m,q} \end{bmatrix} \quad (9)$$

is a matrix of size  $(2K-L+2) \times L$ , where  $L$  is called the pencil parameter. In [13], it is stated that if the value of  $L$  is selected from a certain range, the variance of the estimation results will be minimal. Such a range depends on the snapshot size, which is then translated to our case as

$$(2K+1)/3 \leq L \leq (2K+1)/2. \quad (10)$$

Here, the value of  $L$  will be selected on the basis of the simulation results for this range.

Then,  $\mathbf{Y}^R$  is obtained by reducing the rank of  $\mathbf{Y}$  to  $N_U$ , which is the number of significant sinusoids in the data. This is based on singular-value decomposition as follows. Suppose that  $\mathbf{Y}$  can be expressed as

$$\mathbf{Y} = \mathbf{U}\mathbf{S}\mathbf{V}^H, \quad (11)$$

where  $(\cdot)^H$  denotes the matrix conjugate and transpose,  $\mathbf{U}$  and  $\mathbf{V}$  are unitary matrices, composed of the eigenvectors of  $\mathbf{Y}\mathbf{Y}^H$  and  $\mathbf{Y}^H\mathbf{Y}$ , respectively, and  $\mathbf{S}$  is a diagonal matrix containing the singular values of  $\mathbf{Y}$ . Then,

$$\mathbf{Y}^R = \mathbf{U}\mathbf{S}^R\mathbf{V}^H, \quad (12)$$

where  $\mathbf{S}^R$  is obtained from  $\mathbf{S}$  by setting all the singular values in  $\mathbf{S}$  that are smaller than  $\rho s_{\max}$  to zero, where  $\rho$  is a small positive parameter ( $0 < \rho < 1$ ), and  $s_{\max}$  is the maximum singular value in  $\mathbf{S}$ . Hence,  $N_U$  equals the rank of the resulting  $\mathbf{S}^R$ . A suitable value of  $\rho$  depends on how often and by how much the direct-path amplitude is lower than the strongest-path amplitude. It also depends on the MPM performance in separating the paths from others. In addition, it can depend on the additive noise level. However, the noise-level effect may be minimal in practice because the algorithm always obtains the CSI from a detected data packet for which the signal must be of a detectable quality. As the effect of  $\rho$  on the algorithm performance is so

complex analytically, the value selected in this paper will be based on a simulation study.

Then, the frequency values of the  $N_U$  sinusoids are obtained from  $\mathbf{Y}^R$  as follows. First, the eigenvalues of  $\mathbf{Y}_1^+ \mathbf{Y}_2$  are evaluated, where  $(\cdot)^+$  denotes the Moore-Penrose pseudoinverse, and  $\mathbf{Y}_1$  and  $\mathbf{Y}_2$  are matrices of size  $(2K - L + 1) \times M_q L$ , obtained by deleting the last and first rows of  $\mathbf{Y}^R$ , respectively. Then, the  $N_U$  frequency values  $\omega_0, \omega_1, \dots, \omega_{N_U-1}$  are obtained as the angles of the obtained  $N_U$  eigenvalues.

Suppose that the  $N_U$  frequency values  $\omega_0, \omega_1, \dots, \omega_{N_U-1}$  just obtained have been already sorted in descending order. In addition, consider for simplicity that all the  $N_p$  paths in (6) have clearly distinctive delays and considerable amplitudes compared to the amplitude of the noise. Then,  $N_U$  is an estimate of  $N_p$ . In addition, the  $N_U$  frequency values can be considered as they are related with the effective path delays  $t_{n,q}$  by  $\omega_n = -2\pi B t_{n,q} / N$ . Then, the corresponding complex amplitudes  $a_{n,m}$ ,  $0 \leq n < N_U$ , that estimate  $g_{n,q} e^{-j\phi_{n,m,q}}$  are obtained by applying the conventional linear least-squares method [14] to the problem:

$$\begin{bmatrix} e^{-K\omega_0} & e^{-K\omega_1} & \dots & e^{-K\omega_{N_U-1}} \\ e^{(1-K)\omega_0} & e^{(1-K)\omega_1} & \dots & e^{(1-K)\omega_{N_U-1}} \\ \vdots & \vdots & \ddots & \vdots \\ e^{K\omega_0} & e^{K\omega_1} & \dots & e^{K\omega_{N_U-1}} \end{bmatrix} \begin{bmatrix} a_{0,m} \\ a_{1,m} \\ \vdots \\ a_{N_U-1,m} \end{bmatrix} = \begin{bmatrix} H_{-K,m,q} \\ H_{1-K,m,q} \\ \vdots \\ H_{K,m,q} \end{bmatrix}. \quad (13)$$

**Transforming a reflection-rich CFR** Recall that  $N_U$  denotes the number of significant sinusoids for the frequency estimation. Then,  $\sum_{n=1}^{N_U-1} a_{n,m} e^{j\omega_n k}$  approximates (6), where the terms of the shortest path and the AWGN are ignored, i.e.,

$$\sum_{n=1}^{N_U-1} a_{n,m} e^{j\omega_n k} \approx H_{k,m,q} - g_{0,q} e^{-j(2\pi B t_{0,q} k / N + \phi_{0,m,q})} - w_{k,m,q}, \quad (14)$$

or

$$H_{k,m,q} - \sum_{n=1}^{N_U-1} a_{n,m} e^{j\omega_n k} \approx g_{0,q} e^{-j(2\pi B t_{0,q} k / N + \phi_{0,m,q})} + w_{k,m,q}. \quad (15)$$

Therefore, the effective CFR for the  $m$ -th antenna is obtained by first computing the left-hand side of (15), then translating the frequency of the remaining shortest-path term to zero, and finally averaging the result over the frequency domain, i.e.,

$$G_{m,q} = \sum_{k=-K}^K G_{k,m,q} / (2K + 1), \quad (16)$$

where  $G_{k,m,q}$  is obtained by

$$G_{k,m,q} = \left( H_{k,m,q} - \sum_{n=1}^{N_U-1} a_{n,m} e^{j\omega_n k} \right) e^{-j\omega_0 k}. \quad (17)$$

### 2.2.2 Search for the best location

Searching for the best location involves the computation of likelihood-based metrics for locations of interest, and it is equivalent to maximizing the likelihood over the locations. The likelihood to be maximized is defined by

$$u(\zeta) = f(G_{m,q}; \forall(m, q) | \zeta, g_{0,q}^*; \forall q), \quad (18)$$

where  $f(\cdot)$  denotes the probability density function (PDF),  $\zeta$  denotes the location, and  $g_{0,q}^*, \forall q$ , are  $g_{0,q}, \forall q$ , that jointly maximize  $f(G_{m,q}; \forall(m, q) | \zeta, g_{0,q}; \forall q)$ . Assume that the CSI data have been scaled such that the variances of  $w_{k,m,q}, \forall(m, q)$ , are the same. Note that such scaling requires the average noise power or signal-to-noise ratio of every receiver chain to be estimated. However, as the information is generally required also by the MIMO-OFDM receiver, obtaining the information should not involve any overhead. Then, based on (7) and because  $w_{m,q}, \forall(m, q)$ , are zero mean independent and identical complex Gaussian random variables

$$f(G_{m,q}; \forall(m, q) | \zeta, g_{0,q}; \forall q) = \prod_{\forall q} \prod_{\forall m} \mathfrak{N} \left( g_{0,q} e^{-j(2\pi/\lambda)(r_{m,q}^{(\zeta)} - \bar{r}_q^{(\zeta)})}, \sigma^2 \right), \quad (19)$$

where  $\sigma^2$  is the variance of  $w_{m,q}$ ,  $\mathfrak{N}(\mu, \sigma^2)$  is the PDF of a circularly symmetric complex Gaussian random variable with mean  $\mu$  and variance  $\sigma^2$ ,  $\lambda$  is the wavelength of the radio-frequency carrier,  $r_{m,q}^{(\zeta)}$  is the distance from  $\zeta$  to the  $m$ -th antenna of the  $q$ -th AP, and  $\bar{r}_q^{(\zeta)} = \sum_{m=1}^{M_q} r_{m,q}^{(\zeta)} / M_q$ . Then, it can be shown that

$$\arg \max_{\zeta} u(\zeta) = \arg \max_{\zeta} \sum_{\forall q} \left| \sum_{\forall m} G_{m,q} e^{j(2\pi/\lambda)r_{m,q}^{(\zeta)}} \right|^2. \quad (20)$$

Then, to determine the best location, the metric defined as

$$s(\zeta) = \sum_{\forall q} \left| \sum_{\forall m} G_{m,q} e^{j(2\pi/\lambda)r_{m,q}^{(\zeta)}} \right|^2 \quad (21)$$

is computed for every location of interest, and the best location  $\zeta^*$  is obtained as  $s(\zeta^*) = \max_{\zeta} s(\zeta)$ .

## 2.3 Some remarks

### 2.3.1 AOA-based localization

We may note that the location metric (21) is a sum of metrics, each of which is contributed by the data of an AP, i.e.,

$s(\zeta) = \sum_{\forall q} s_q(\zeta)$ , where  $s_q(\zeta) = |\sum_{\forall m} G_{m,q} e^{j(2\pi/\lambda)r_{m,q}^{(\zeta)}}|^2$ . The metric contributed by the data of an AP has an interesting property that may be described as follows. Note that the metric  $s_q(\zeta)$  can be equivalently expressed by  $s_q(\zeta) = |\sum_{\forall m} G_{m,q} e^{j(2\pi/\lambda)[r_{m,q}^{(\zeta)} - r_{1,q}^{(\zeta)}]}|^2$ . Then, since  $r_{m,q}^{(\zeta)} - r_{1,q}^{(\zeta)}$ ,  $\forall m$  will not considerably change if  $\zeta$  moves along on the same AOA to the  $q$ -th AP,  $s_q(\zeta_1) \approx s_q(\zeta_2)$  if  $\zeta_1$  and  $\zeta_2$  are along similar AOAs to the  $q$ -th AP. Then, we can conclude that the metric contributed by the data of an AP contains information of the AOA to the AP.

The usefulness of the effective CFR obtained by (16) may be noted as follows. Thus far, we have assumed that the direct path exists and all paths also have distinctive delays. However, paths can actually have indistinguishable delays. Then, a problem could arise when some scattered paths of considerable amplitudes have delays close to the delay of the direct path, while they also have AOAs considerably different from that of the direct path. In this case, the effective CFR will possibly contain also the AOA information of the scattered paths that can degrade the location estimation of the proposed algorithm. Therefore, the proposed algorithm requires significant scattered paths with delays close to the delay of the direct path to also have AOAs close to the AOA of the direct path. This could be realistic if the placement of the AP antenna array is not close to any significant reflective materials. Such placement also seems to be a good practice for other AOA-based localization systems.

### 2.3.2 Effect of MT velocity

It may be interesting to assess the effect of the MT velocity on the performance of the proposed algorithm. In this regard, we consider that there are two issues caused by MT movement that may affect the performance. One issue is the location shift of the MT that may change the real multipath configuration of the channel during the OFDM training symbol. The other issue is the Doppler shift of the direct-path term in the estimated CSI. The location shift should be of no concern because the duration of the training symbol is just 4  $\mu$ s, which means that a moving speed of 900 km/h is required to observe a location shift of 1 mm. The 1-mm shift does not seem to significantly change the multipath configuration, and the 900-km/h speed is infeasible in indoor environments.

Regarding the Doppler shift, it should be noted that movement of the MT during a packet transmission would cause a direction-dependent spectral shift of the radiating wave. Hence, the spectral shift of one transmission path arriving at the receiver could be different from the spectral shifts of other paths. This effect is not as simple as that of the local oscillator frequency offset between the transmitter and the receiver, where the effect is equivalent to causing identical spectral shifts for all paths. However, the

direction-dependent spectral shifts could only change the phases of the sinusoidal terms in (6) and therefore could not affect the frequency estimation of the MPM. In addition, the spectral shift of the direct-path term could only rotate  $g_{0,q}$  in (6) through a certain angle and therefore could not change the MT location information in  $\phi_{0,m,q}$ ,  $1 \leq m \leq M_q$ .

However, the Doppler shift is known to cause inter-carrier interference in OFDM data detection. It will also affect the CSI estimation that is conventionally based on detecting the data carried by the training symbol. For a successfully detected data packet, we can expect that such interference is insignificant. Therefore, in this paper, we assume that the effect is negligible. Nevertheless, we believe that it merits a detailed analysis that should be conducted in a separate study.

### 2.4 CRLB for two-dimensional systems with linear-type arrays

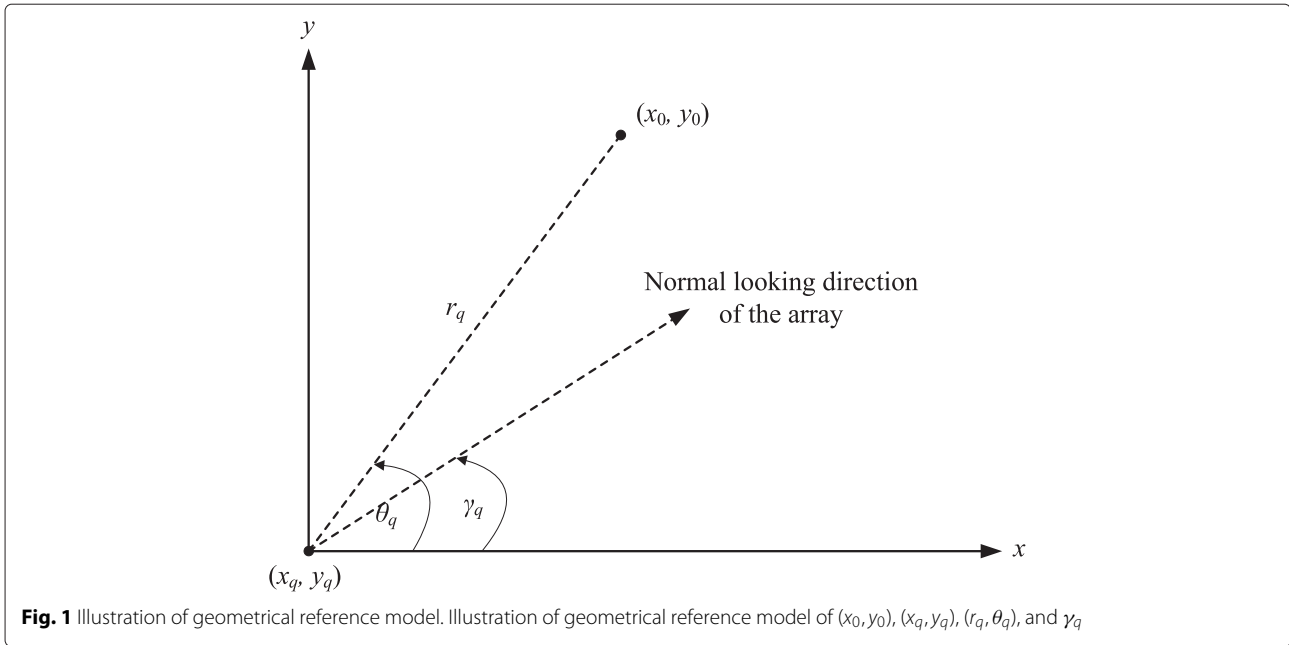
For benchmarking the performance of the location estimators based on (7), we obtain the Cramer-Rao lower bound (CRLB) [15], which is the variance of the estimation error of a minimum variance unbiased estimator. This is done on the basis of the following considerations. First, we model the observation of the estimator as a real vector:

$$\mathbf{X} = [\mathbf{O}_1^T \quad \mathbf{O}_2^T \quad \cdots \quad \mathbf{O}_Q^T]^T, \quad (22)$$

where  $Q$  is the number of APs,  $(\cdot)^T$  denotes the matrix transpose, and

$$\mathbf{O}_q = \begin{bmatrix} |g_{0,q}| \cos(\phi_{0,1,q} - \angle g_{0,q}) + \Re(w_{1,q}) \\ -|g_{0,q}| \sin(\phi_{0,1,q} - \angle g_{0,q}) + \Im(w_{1,q}) \\ |g_{0,q}| \cos(\phi_{0,2,q} - \angle g_{0,q}) + \Re(w_{2,q}) \\ -|g_{0,q}| \sin(\phi_{0,2,q} - \angle g_{0,q}) + \Im(w_{2,q}) \\ \vdots \\ |g_{0,q}| \cos(\phi_{0,M_q,q} - \angle g_{0,q}) + \Re(w_{M_q,q}) \\ -|g_{0,q}| \sin(\phi_{0,M_q,q} - \angle g_{0,q}) + \Im(w_{M_q,q}) \end{bmatrix}. \quad (23)$$

We restrict the analysis to only the case in which each AP antenna array is of linear type. Then, we base the computation on the following geometrical reference model. Denote the location of the array center of the  $q$ -th AP in the Cartesian coordinate system as  $(x_q, y_q)$  and that of the MT as  $(x_0, y_0)$ . The locations are related using the polar coordinate system as  $(r_q, \theta_q)$ , as shown in Fig. 1. Define a normal looking direction of an antenna array as a main radiation direction when the phase shifts of all the antenna elements are zero. While the linear antenna array of an AP has two normal looking directions, we shall be interested in only the one that is closest to the direction of arrival of the MT. For the  $q$ -th AP, we denote the counter-clockwise angle of the normal looking direction relative to the  $x$ -axis



as  $\gamma_q$ . For example, if the array elements of the  $q$ -th AP are placed along the  $x$ -axis in Fig. 1,  $\gamma_q$  will be  $\pi/2$ . Then, assuming that the spacing between the antenna elements in each array is  $d$  and  $r_q \gg d$ ,  $\phi_{0,m,q}$ ,  $\forall(m, q)$ , can be approximated by

$$\phi_{0,m,q} = \frac{2\pi}{\lambda} (m - (M_q + 1)/2) d \sin(\theta_q - \gamma_q). \quad (24)$$

Based on [15], the CRLB can be computed by

$$\text{CRLB}(\hat{\zeta}) = [\mathbf{I}^{-1}]_{1,1} + [\mathbf{I}^{-1}]_{2,2}, \quad (25)$$

where  $[\mathbf{K}]_{i,j}$  denotes the  $(i, j)$  element of matrix  $\mathbf{K}$  and  $\mathbf{I}$  is the Fisher information matrix:

$$[\mathbf{I}]_{i,j} = \frac{2}{\sigma^2} \frac{\partial \boldsymbol{\mu}^T}{\partial u_i} \frac{\partial \boldsymbol{\mu}}{\partial u_j}, \quad (26)$$

where  $\boldsymbol{\mu}$  is the mean of  $\mathbf{X}$ , and  $(u_1, u_2, \dots, u_{2Q+2}) \doteq (x_0, y_0, |g_{0,1}|, \angle g_{0,1}, \dots, |g_{0,Q}|, \angle g_{0,Q})$ . However, following [16], the CRLB may be also computed by

$$\text{CRLB}(\hat{\zeta}) = [\mathbf{I}_e^{-1}]_{1,1} + [\mathbf{I}_e^{-1}]_{2,2}, \quad (27)$$

where  $\mathbf{I}_e$  is the equivalent Fisher information matrix obtained as follows. Let

$$\mathbf{I} = \begin{bmatrix} \mathbf{A} & \mathbf{B} \\ \mathbf{B}^T & \mathbf{C} \end{bmatrix}, \quad (28)$$

where the sizes of matrices  $\mathbf{A}$ ,  $\mathbf{B}$ , and  $\mathbf{C}$  are  $2 \times 2$ ,  $2 \times 2Q$ , and  $2Q \times 2Q$ , respectively. Then,  $\mathbf{I}_e$  can be computed by

$$\mathbf{I}_e = \mathbf{A} - \mathbf{B}\mathbf{C}^{-1}\mathbf{B}^T. \quad (29)$$

Noting that  $\partial \theta_q / \partial x_0 = -(\sin \theta_q) / r_q$  and  $\partial \theta_q / \partial y_0 = (\cos \theta_q) / r_q$ , we then apply these two relations and (22), (23), and (24) to derive the elements of  $\mathbf{A}$ ,  $\mathbf{B}$ , and  $\mathbf{C}$ .

Accordingly, after arranging the terms, we obtain  $\mathbf{B}$  as a zero matrix, and therefore,  $\mathbf{I}_e = \mathbf{A}$ , which can be expressed by

$$\mathbf{I}_e = \frac{1}{\sigma^2} \sum_{q=1}^Q |g_{0,q}|^2 \frac{M_q(M_q^2 - 1)}{6} \left( \frac{2\pi d \cos(\theta_q - \gamma_q)}{\lambda r_q} \right)^2 \mathbf{p}^{(\theta_q)} \mathbf{p}^{(\theta_q)T}, \quad (30)$$

where

$$\mathbf{p}^{(\theta_q)} = [\sin(\theta_q) \quad -\cos(\theta_q)]^T. \quad (31)$$

We may use (27) and (30) to compute the CRLB as a function of  $g_{0,q}$ ,  $1 \leq q \leq Q$ , which are random variables. In this paper, by considering such variability, the CRLB is then obtained by averaging the computed CRLBs across the simulated values of  $\{g_{0,q} | 1 \leq q \leq Q\}$ .

### 3 Numerical results and discussions

#### 3.1 Multipath propagation model

In this paper, we estimate the performance of the proposed algorithm on the basis of computer simulation using statistical indoor channel models. In addition, because our algorithm is AOA-based, we require a relevant channel model to provide specifications of the AOA characteristics in addition to the power delay profile of the multipath. As we find that only the IEEE 802.11 TGN channel models [17] are available in detail and meet our requirements, we base our performance evaluation on only such models.

Let us briefly describe the major characteristics of the models as follows. In a TGN channel model, a non-line-of-sight (NLOS) model is defined by delay taps, with each

tap representing the contribution of scattered paths of the same delay. The delay taps are grouped into clusters such that scattered paths within the same cluster possess the same random characteristics of the AOA to the receiver. In other words, the AOAs of scattered paths of a cluster are obtained as follows. First, the mean AOA is drawn from a uniform distribution over  $[0, 2\pi)$ . Then, the AOA of each scattered path is drawn from a Laplacian distribution according to the obtained mean and the angular spread (AS), i.e., the standard deviation, specific to the cluster. The amplitude of a scattered path is a complex Gaussian random variable, with the magnitude being a Rayleigh distribution. The number of clusters, power delay profile, and AS of each cluster are specific to model subtype, e.g., the number of clusters is three for model D. The total received power in an NLOS model is also subjected to path loss, which includes a log-normal shadowing effect and is specific to the model subtype. The TGn channel modeling also provides a line-of-sight (LOS) model for each model subtype, which is relevant to our case where the localization algorithm requires the existence of LOS. In a TGn channel model, an LOS model of a subtype is simply obtained by adding an LOS component to the first arriving tap of the corresponding NLOS model. However, the addition is done according to a first-tap k-factor, i.e., the ratio of the LOS power to the average power of the NLOS first tap, which is specific to the model subtype. The TGn channel modeling does not use a large first-tap k-factor for any model subtype because changing from the NLOS model to the LOS model of the same subtype will slightly reduce the root-mean-square (RMS) delay spread of the channel (see Table 1).

However, we note that the described LOS model consists of LOS and NLOS parts, with the first tap of the NLOS part being set to have the same delay as (but arbitrarily different AOA from) the LOS. This seems to be unrealistic if the placement of the AP antenna array is not close to any significant reflective materials. Such placement seems to be also a good practice for other AOA-based localization systems. Assume that such placement has been done successfully for every array, although

absorptive materials may be required in some cases. Then, it would be more realistic if a scattered path with a delay close to that of the LOS also had its AOA statistically close to that of the LOS. Accordingly, we modify the TGn channel models for our purpose by (i) setting the mean AOA of the NLOS first tap to equal the AOA of LOS and (ii) introducing a new parameter  $\sigma_0$  as the AS of the NLOS first tap. The impact of this parameter on the algorithm performance will be studied by simulation.

The TGn channel models include six model subtypes with RMS delay spread in the range of 0 to 150 ns. We use the LOS models D and E in this paper because according to [18], the associated delay spreads are representative of typical office environments for model D and typical large open spaces and office environments for model E. In addition, such environments are expected to be targets of a wide range of indoor location-based services. The characteristics of the two models in terms of the first-tap k-factor, the RMS delay spread, and the maximum delay spread ( $t_{N_p-1,q} - t_{0,q}$ ) are summarized in Table 1, while additional details can be found in [17]. Note that each LOS model is multipath-rich while having a direct path that is nondominant because changing from the NLOS model to the LOS model of the same subtype can just slightly reduce the RMS delay spread of the channel.

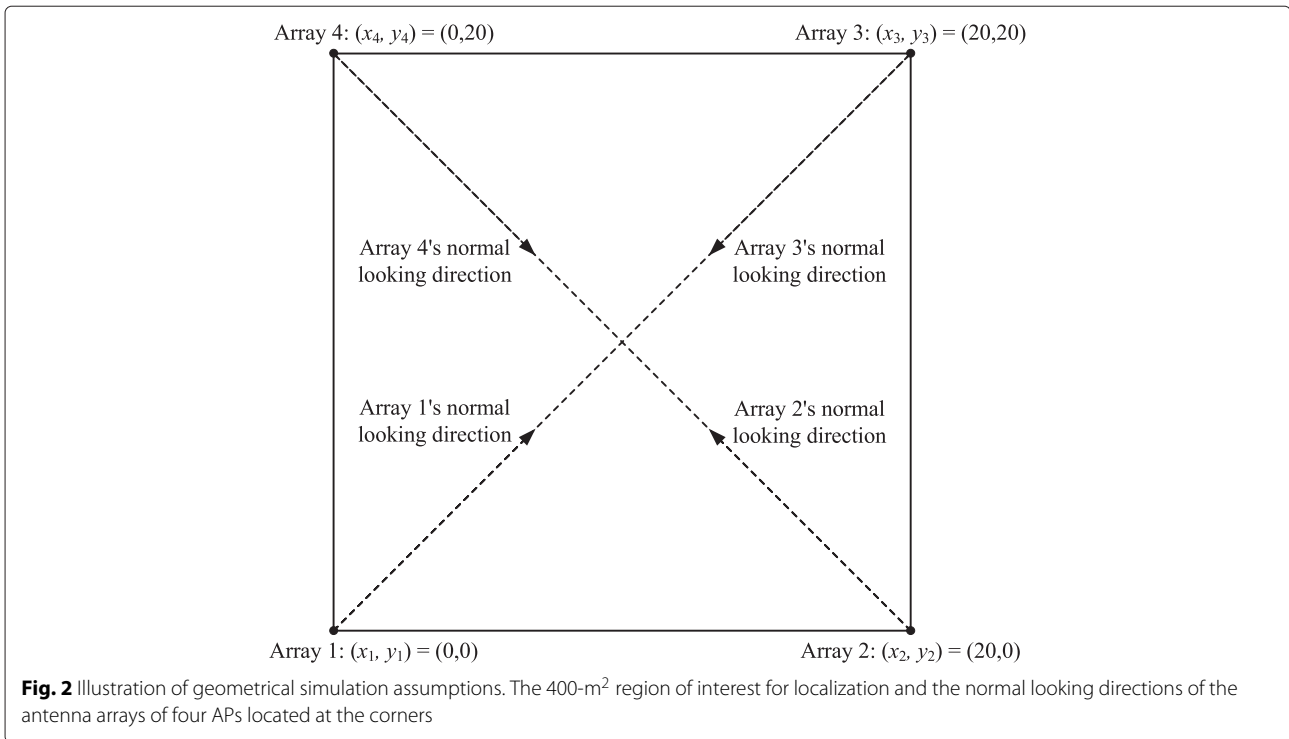
### 3.2 Common assumptions and search method

The performance of the proposed method is evaluated with geometrical assumptions as shown in Fig. 2, illustrating the region of interest for localization, which is a square having an area of 400 m<sup>2</sup> and the normal looking directions of the antenna arrays of four APs located at the corners of the square. Each antenna array is of linear type with half-wavelength spacing between elements. A carrier frequency of 5 GHz is assumed. In addition, an antenna gain of 0 dB is assumed for the MT antenna as well as for each array element of an AP. Further, it is assumed that the variance of the CSI estimation error depends only on the system noise, i.e.,  $E[|H_{k,m,q} - w_{k,m,q}|^2]/E[|w_{k,m,q}|^2]$  equals the average signal-to-noise ratio per OFDM subcarrier. Regarding the OFDM signal models [1], we will consider only the 40-, 80-, and 160-MHz models, as they should be sufficient for demonstrating the performance with regard to the bandwidth.

In this paper, the search for the best location on the basis of the metric of (21) is conducted in three rounds. In the first round, the metrics are computed for regular grid points over the 400-m<sup>2</sup> square region with a grid-point spacing of 1 m, and the first-round optimum location is then determined. In the  $(n + 1)$ -th round, the metrics are computed for regular grid points over the  $(l_n^2)$ -m<sup>2</sup> square region centered at the  $n$ -th round optimum location with a grid-point spacing of  $l_n/20$ , and the  $(n + 1)$ -th-round optimum location is then determined, where  $l_n/2$  equals the

**Table 1** NLOS and LOS characteristics of models D and E of [17]

		Model D	Model E
First-tap k-factor (dB)	NLOS	$-\infty$	$-\infty$
	LOS	3	6
RMS delay spread (nm)	NLOS	50	99
	LOS	47	95
Maximum delay spread (nm)	NLOS	390	730
	LOS	390	730



grid-point spacing in meters for the  $n$ -th round. Note that the grid-point spacing for the last round, representing the effective resolution of the search space, is  $10^{-2}$  m.

### 3.3 Selection of algorithm parameters

The performance of the proposed algorithm depends on its parameters  $L$  and  $\rho$ . We realize that obtaining optimal values of the parameters may require a separate elaborate study. In this paper, we only select certain values for demonstrating the basic working performance of the proposed algorithm and for comparing the proposed algorithm with previous methods. This is done for each standard signal model [1] as follows.

First, we select a tentative value of  $L$  to be the middle value of the range (10). Therefore, the selected values for the 40-, 80-, and 160-MHz OFDM signal models are 49, 102, and 209, respectively.

Then, a tentative value of  $\rho$  is selected from the simulation results as shown in Fig. 3. The results show the root-mean-square error (RMSE) versus  $\rho$  with OFDM signal bandwidth ( $B$ ) and number of antennas per AP ( $M_q = M, \forall q$ ) as parameters. The RMSE is obtained from 1000 independent samples, based on the following assumed typical conditions. The MT transmitted power is 10 dBm, the AP receiver noise figure (NF) is 4 dB, and the LOS model D is used with  $\sigma_0 = 4^\circ$ . In addition, the MT is uniformly and randomly located in the 400-m<sup>2</sup> region, except the locations that are close to the center of an antenna array by less than 1 m. All the RMSE values shown

in the figure are based on same test data, defined by the drawn MT locations and channel characteristics. According to the results, the selected values of  $\rho$  are 1/32 for the 40- and 80-MHz models and 1/16 for the 160-MHz model, as they represent a rough approximation of the optimal values for the assumed conditions.

Then, we iterate the simulation experiments by fixing the value of  $\rho$  to the tentative one and performing simulations for evaluating the performance in terms of  $L$ . According to the results, the performance does not vary significantly with  $L$ . Therefore, the tentative values of  $L$  and  $\rho$  stated above are adopted in this paper.

### 3.4 Implications of $\sigma_0$ and CSI interpolation

We also study the implications of the AS of the NLOS first tap and CSI interpolation. The localization performance is evaluated with the same assumptions as in Section 3.3, except that  $L$  and  $\rho$  are set to be the selected values and  $\sigma_0$  is now variable. The performance is also evaluated for two cases. One is based on using discontinuous CSI as input data and using linear interpolation to obtain contiguous CSI as proposed. The other is based on using contiguous CSI as input data, assuming that the used OFDM subcarriers are already contiguous. For a value of  $\sigma_0$ , the performance results for both cases of CSI data are based on the same test data, defined by the drawn MT locations and channel characteristics. It may be noted from the results shown in Fig. 4 that the localization performance of both cases is similar, although using discontinuous CSI



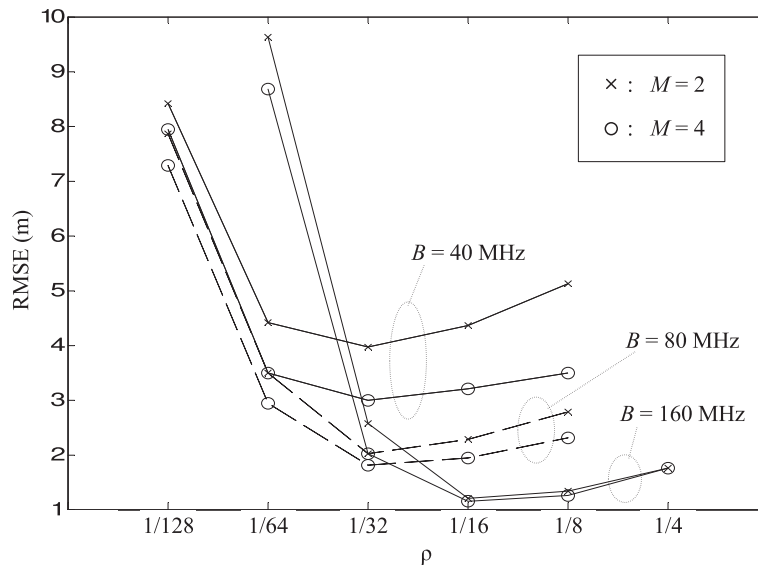


**Fig. 3** Average localization error in terms of  $\rho$ . Root-mean-square error versus  $\rho$  with OFDM signal bandwidth and number of antennas per AP as parameters

with linear interpolation leads to slightly worse performance. Hence, we may conclude that linear interpolation is effective in mitigating the problem of CSI discontinuity in the proposed algorithm. The results also show that the RMSE values when  $\sigma_0 = 0^\circ, 4^\circ, 8^\circ,$  and  $16^\circ$  for both cases are around 0.7, 1.1, 1.6, and 2.7 m, respectively. Hence, controlling  $\sigma_0$  to be small based on the placement of the antenna arrays as mentioned in Section 3.1 is very important for realizing good performance of the proposed algorithm.

**3.5 Comparison with other methods**

The performances of the proposed method, the RSSI-based method [8], and the CSI-based method [9] were compared under the same statistical channel conditions. The CSI-based method [9] and the RSSI-based method are similar but differ in terms of the observation data that they use. The RSSI-based method uses the RSSI as observation data, whereas the CSI-based method [9] uses a norm computed from the CSI as observation data. We will refer to the RSSI-based method [8] and the CSI-based

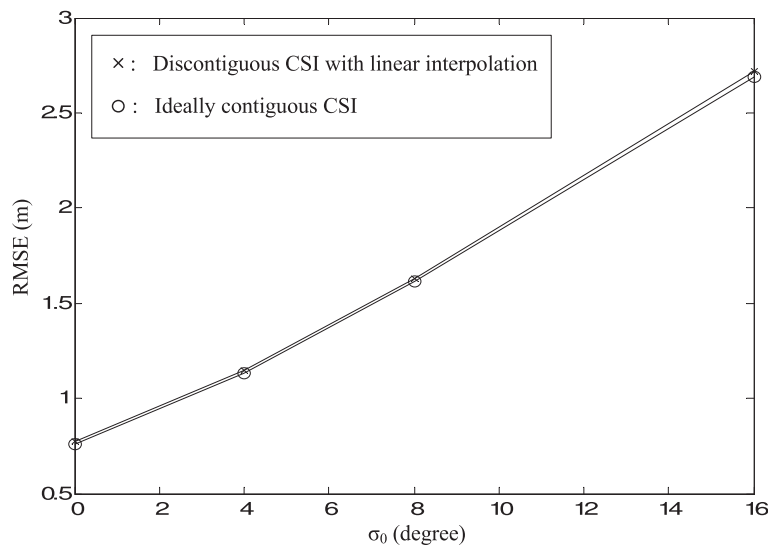


**Fig. 4** Average localization error in terms of  $\sigma_0$ . Root-mean-square error versus  $\sigma_0$  for two cases of CSI data

method [9] as the RSSI method and the CSI norm method, respectively. Both methods require the localization algorithm to be trained before use or testing. In the training process, usually referred to as fingerprinting, the PDF of the observation data conditioned on the MT location is obtained from the training data for each reference location. In the use phase, the location is determined as a weighted average of the reference locations according to the observation data and the trained model. For the performance comparison, the LOS models D and E are used with the following simulation conditions. The MT transmitted power is 10 dBm, the AP receiver NF is 4 dB, and each LOS model has  $\sigma_0 = 4^\circ$ . In addition,  $B = 160$  MHz and  $M = 2$ . The MT locations for testing are rectangular grid points spanning the 400-m<sup>2</sup> region with a grid-point spacing of 1 m, except for the center points of the four antenna arrays. The set of reference locations for the RSSI and CSI-norm methods is the same as the set of MT locations for testing. Because the RSSI and CSI-norm methods assume observation data from a single antenna, the RSSI and CSI-norm averaged across the antennas in the array are respectively used as the observation data for the two methods in this paper. The training data for each reference location consist of 500 independent samples of the observation data, while the test data for each grid point consist of 10 other independent samples.

Figures 5 and 6 show the results of the cumulative distribution function (CDF) according to models D and E, respectively. It can be noted that the proposed algorithm clearly outperforms the other two methods in both

channel models. Note that the RSSI and CSI-norm methods are not generally designed to model both small-scale and large-scale fading effects. They are designed to model only the variabilities of small-scale fading conditioned on a fixed large-scale fading condition because when a significant object moves in the environment and changes the large-scale fading condition, the methods usually need to be retrained for maintaining the performance. In the simulation environment of this study, different samples of observation data correspond to totally independent fading conditions. Therefore, the two methods cannot perform well in this simulation experiment. The figures also show that the performance of the proposed method improves when changing from model D to model E, possibly because of the stronger LOS component in model E.

### 3.6 Effect of infrastructure conditions

Figure 7 shows the results of the localization performance in terms of the signal-to-noise condition, signal bandwidth, and number of antennas per AP. The localization performance is evaluated with the same assumptions as in Section 3.3, except that  $L$  and  $\rho$  are set to be the selected values and the MT transmitted power is varied over the range of  $-20$  to  $20$  dBm. All the RMSE values shown in the figure are based on the same test data, defined by the drawn MT locations and channel characteristics. The figure shows that the localization performance improves with increasing MT transmitted power, but the improvement is saturated when the power increases over around

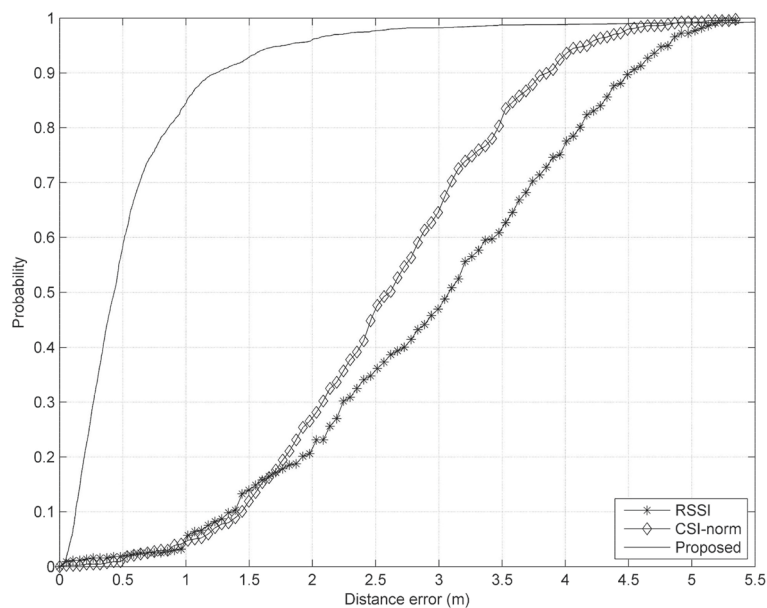


**Fig. 5** Performance comparison according to channel model D. CDF of localization errors for the RSSI, CSI-norm, and proposed methods according to channel model D

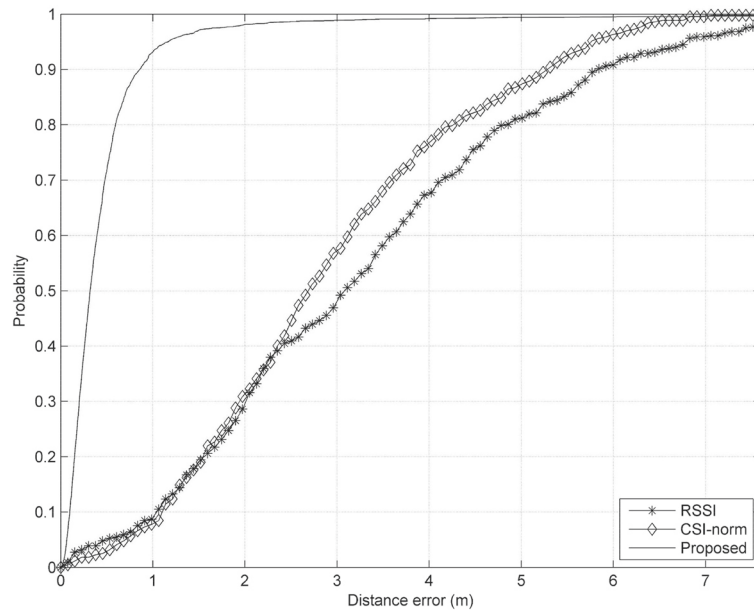


**Fig. 6** Performance comparison according to channel model E. CDF of localization errors for the RSSI, CSI-norm, and proposed methods according to channel model E

10 dBm. We believe that the performance saturation could be mainly due to residual contributions from scattered paths that still remain in the effective CFR. Note that we could expect such contributions to be smaller by having richer observation data for the multiple-sinusoid parameter estimation process of the proposed algorithm. This is supportive of the results shown by the figure, where the saturated performance improves with increasing  $B$  or

$M$ . The saturated performance, when the MT transmitted power equals 10 dBm, is summarized in Table 2. The table lists numerical values of the RMSE in meters and also in percent maximal length of a straight line within the localization region, in order to illustrate how the errors are related to the dimension of the localization region. Note that the maximal length is considered to be  $20\sqrt{2}$  m. Comparing the performance improvement as a result of

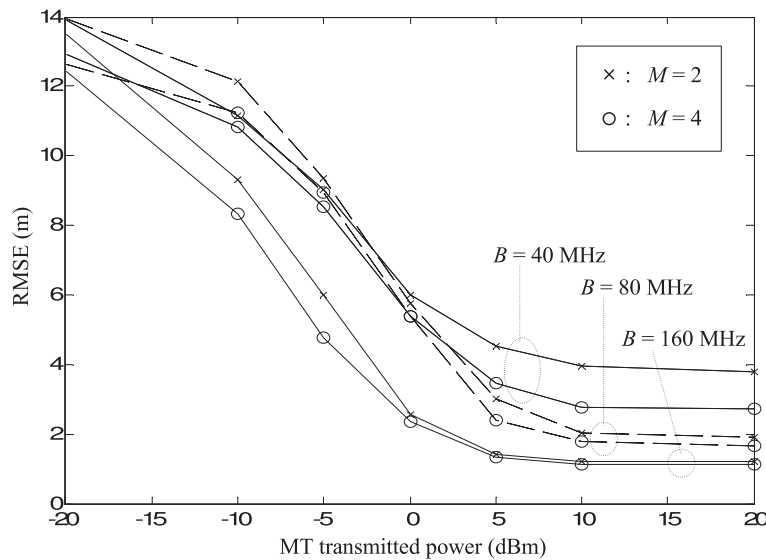


**Fig. 7** Average localization error in terms of the signal-to-noise condition, signal bandwidth, and number of antennas per AP. Root-mean-square error versus MT transmitted power with OFDM signal bandwidth and number of antennas per AP as parameters

**Table 2** Localization performance in terms of  $B$  and  $M$  when the MT transmitted power is 10 dBm, expressed as root-mean-square error in meters and also in percent maximal length of a straight line within the localization region

	$M = 2$	$M = 4$
$B$ (MHz)		
40	3.9 m; 13.79 %	2.8 m; 9.90 %
80	2.0 m; 7.07 %	1.8 m; 6.36 %
160	1.2 m; 4.24 %	1.1 m; 3.89 %

changing from  $M = 2$  to  $M = 4$  for the three cases of  $B$  shown in the table, we can see that the improvement decreases with increasing  $B$ .

Figure 8 compares the results of Fig. 7 and the CRLB when  $B = 160$  MHz. The important points to be noted are as follows. The CRLB performance always improves steadily with increasing MT transmitted power. The performance of the proposed algorithm is much worse than that of the CRLB in all the cases. This large performance gap is expected because the CRLB here is based on the observation data modeled by (7), which is free of scattered-path contributions, and the CRLB result corresponds to an optimal unbiased estimator. The source of impairment of the CRLB results is only the AWGN.

It is also interesting to see how the proposed method performs in terms of the MT location and the number of usable APs. Figures 9, 10, 11 and 12 show the simulation results with the same assumptions as in Section 3.5, except that the test data for each grid point here consist of 30 independent samples and only model D is used.

It can be noted from Fig. 9 that the 90 % confidence level error bound, i.e., the error when the cumulative probability

is 0.9, increases approximately from 1.2 to 1.6 and 3.5 m when the number of usable APs is reduced from 4 to 3 and 2, respectively. The performance seems to degrade steadily if the number of usable APs is greater than two. However, the performance with two APs is still better than the performances of the RSSI and CSI-norm methods with four APs, as shown in Fig. 5, from which we may note that the 90 % confidence level error bounds are around 4.5 and 3.8 m for the RSSI and CSI-norm methods, respectively. For the proposed method, the preferable number of usable APs seems to be three or greater, while having only two usable APs may still be viable in some applications.

Regarding the localization performance in terms of the MT location, it is interesting to note from Fig. 10 that the RMSE is locally large for locations on the line connecting the two usable APs. This can be explained by noting that the locations on such a line correspond to the case where the equivalent Fisher information matrix expressed in (30) is singular. Intuitively, the singularity indicates that the available information is not sufficient for estimation, i.e., the location information contribution in the observation data is not sufficient for deducing a location. Therefore, the localization performance in the singularity case here is extremely vulnerable to the AWGN. It may be noted from Figs. 11 and 12 that having more usable APs effectively relieves the singularity problem, especially for locations farther away from the two underlying APs. In contrast, having more usable APs is less effective in relieving the problem for locations close to an AP, possibly because the equivalent Fisher information matrix for such a location is largely dominated by only the contribution of that AP.

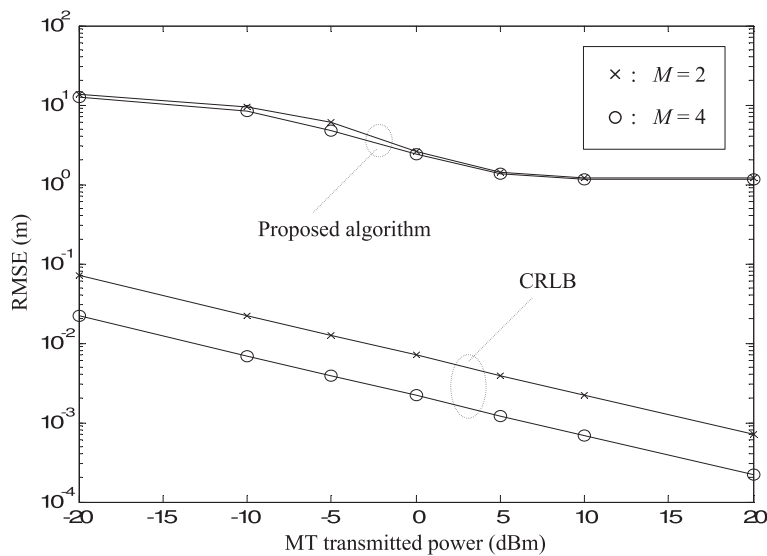


**Fig. 8** Comparison with CRLB when  $B = 160$  MHz. Root-mean-square error versus MT transmitted power with number of antennas per AP as a parameter when  $B = 160$  MHz

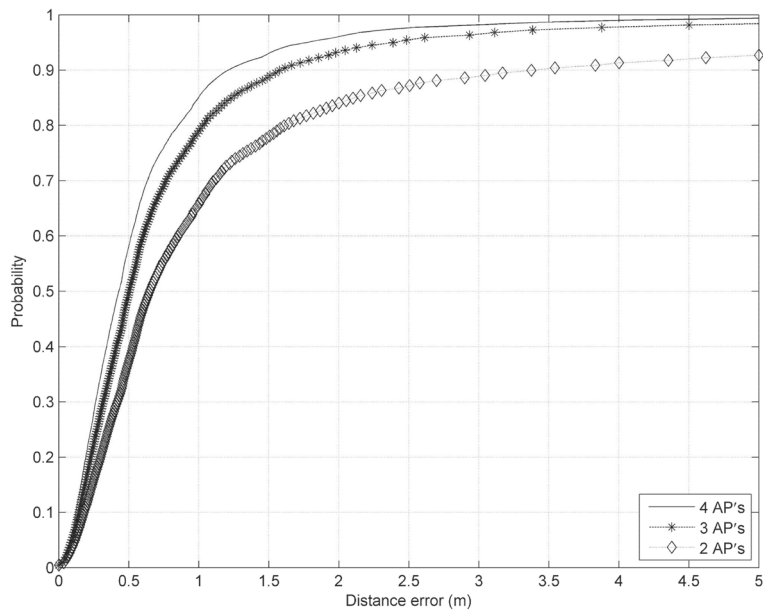


**Fig. 9** Performance in terms of the number of usable APs. CDF of localization errors in terms of the number of usable APs

**4 Recommendations for further study**

The purpose of this paper is to introduce a new algorithm for indoor localization and to demonstrate the potential superiority of the proposed algorithm over previous approaches to the same problem. We believe that the issues listed below merit further investigation.

- *Validation with real measurements:* In this paper, the localization performance of the proposed algorithm was evaluated on the basis of statistical indoor

channel models specifically obtained for benchmarking data communication systems. It is much more relevant to evaluate the performance on the basis of real measurements or a statistical indoor channel model specifically obtained from real measurements for benchmarking AOA-based localization systems. Therefore, performance validation with real measurements is very important.

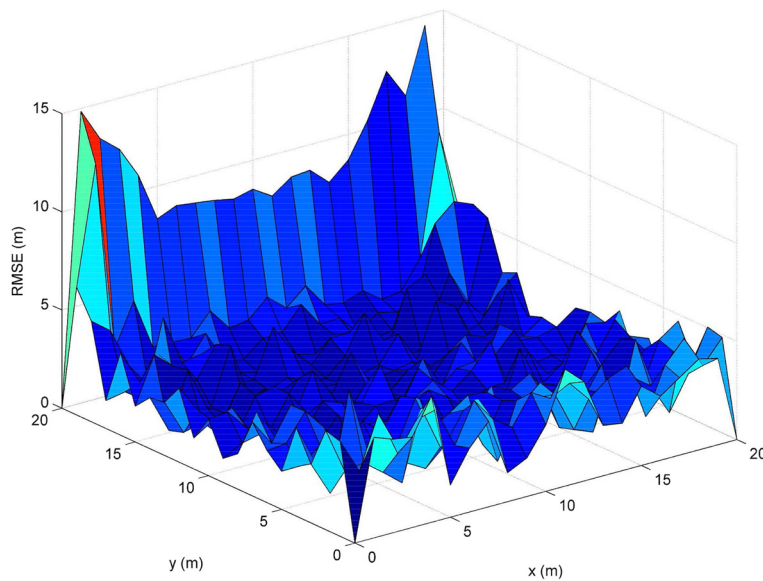


**Fig. 10** Average localization error in terms of the MT location based on two usable APs. Root-mean-square error versus MT location when only two APs located at (0,20) and (20,20) m are usable

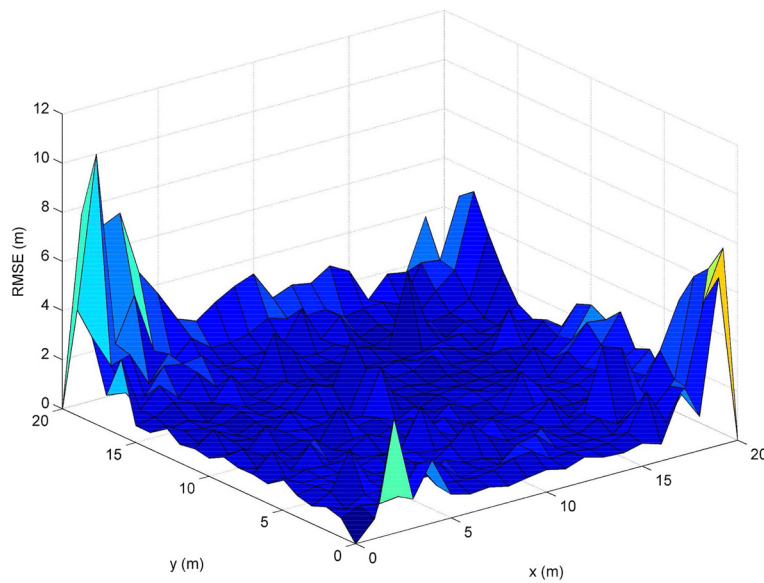


**Fig. 11** Average localization error in terms of the MT location based on three usable APs. Root-mean-square error versus MT location when only three APs located at (0,20), (20,20), and (20,0) m are usable

- *Other super-resolution methods:* Estimating the frequencies of all the sinusoids in the CFRs plays a major role in obtaining an effective CFR for the proposed algorithm. Although the MPM is used in this paper because it directly addresses the problem of interest, we believe that other super-resolution methods should also be studied in this regard.
- *Using a priori knowledge in estimation:* In this paper, estimating the parameters of all the sinusoids in the CFRs plays a major role in obtaining an effective CFR. Such estimation has been performed without considering a priori knowledge about the parameters, i.e., their statistical models. Note that such knowledge may be used to improve the estimation performance

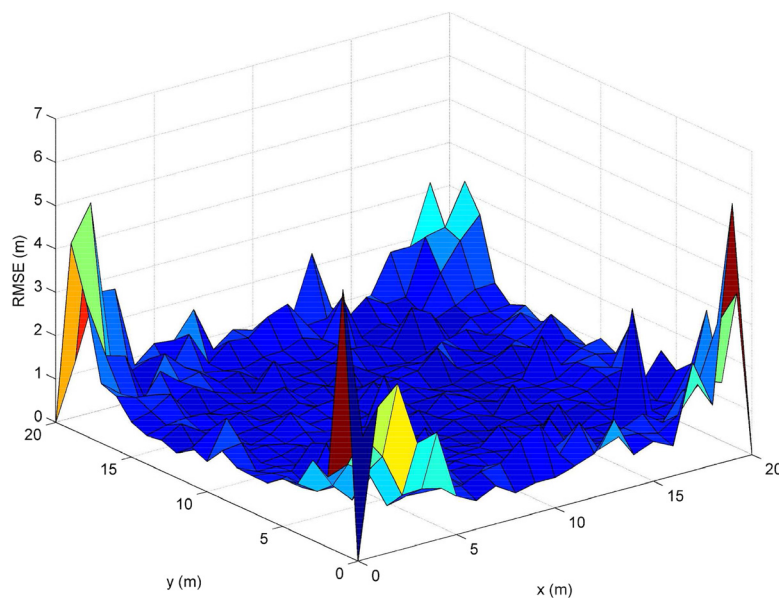


**Fig. 12** Average localization error in terms of the MT location based on four usable APs. Root-mean-square error versus MT location when all four APs are usable



in general, as discussed in [16]. Applying such knowledge to the proposed algorithm is an interesting direction for further study.

- **Optimal parameters for the algorithm:** In this paper, the values of the algorithm parameters  $L$  and  $\rho$  were selected for simply demonstrating the basic working performance of the proposed algorithm. Actually, the optimal values could depend on variable conditions of the radio channel and infrastructure. These effects are also worthy of further study.
- **Problem of NLOS:** In addition to bandwidth availability and multiple-antenna configuration, an essential requirement for the proposed algorithm to work is the availability of LOS in the radio channel. In this regard, the availability required is just sufficient for triangulation. This requirement is the same as for the ultrawideband-based localization regime [19, 20]. Several methods for mitigating the problem of LOS availability have been presented in the literature. These methods are based on the detection of channel condition. By applying the detection of channel condition, we may simply ignore an AP if the detection result declares unavailability of LOS. We could then expect performance degradation on the basis of the results shown in Fig. 9, or encounter an outage if the number of usable APs is less than two. We note that the signal processing results obtained using the proposed method are employed as observation data for the detection of channel condition. However, a detailed study of such detection is beyond the primary scope of the present paper and it is therefore recommended for future work.
- **AOA bias induced by diffraction:** In the present study, the effect of diffraction caused by building components, such as walls, is ignored. If not properly managed, this effect may degrade the performance of the proposed algorithm by introducing a bias into the AOA of a direct path, as well as the performance of the ultrawideband-based localization regime by introducing a bias into the time of arrival of a direct path. Therefore, further investigation is required to efficiently mitigate such a bias.
- **MT velocity effect:** As discussed in Section 2.3.2, a detailed analysis of the effect of MT velocity on the localization performance should be carried out in a future study.
- **Simple way to obtain the effective CFR:** Note that  $a_{n,m}$  obtained using the proposed algorithm by solving (13) is an estimation of  $g_{n,q}e^{-j\phi_{n,m,q}}$ . Therefore, according to (7),  $a_{0,m}$  is also an estimation of  $G_{m,q}$ . Then, it might be better to save computation by using  $a_{0,m}$  as  $G_{m,q}$ , instead of obtaining  $G_{m,q}$  from (16). This issue also requires further investigation in

order to observe its possible effects on the localization performance.

## 5 Conclusions

A new localization method based on an asynchronous network of MIMO-OFDM access points was proposed. This method can be implemented on WLANs of a current standard without affecting their protocol structures. The method involves first obtaining effective CFRs, in which irrelevant contributions from scattered paths and the uncertainty of the OFDM time synchronizer are minimal, and then searching for the most likely location. The proposed method does not require a training process for adaptation to ever-changing environments. The availability of direct paths is sufficient for triangulation, as in the ultrawideband-based localization regime. Further, significant scattered paths with delays close to the delay of the direct path are required to have AOAs close to the AOA of the direct path.

### Competing interests

The authors declare that they have no competing interests.

### Author details

<sup>1</sup>National Electronics and Computer Technology Center (NECTEC), National Science and Technology Development Agency (NSTDA), 112 Thailand Science Park, Phahonyothin Road, Pathum Thani 12120, Thailand. <sup>2</sup>School of Electrical and Electronics Engineering, Chung-Ang University, Seoul, South Korea.

Received: 15 July 2015 Accepted: 31 May 2016

Published online: 10 June 2016

### References

1. IEEE Std 802.11ac - 2013, IEEE Standard for Information Technology—Telecommunications and information exchange between systems—local and metropolitan area networks—specific requirements, Part 11: wireless LAN medium access control (MAC) and physical layer (PHY) specifications, Amendment 4: enhancements for very high throughput for operation in bands below 6 GHz. (The Institute of Electrical and Electronics Engineers, Inc., New York, NY, USA, 2013)
2. H Liu, H Darabi, P Banerjee, J Liu, Survey of wireless indoor positioning techniques and systems. *IEEE Trans. Syst. Man, Cybernetics—Part C: Appl. Rev.* **37**(6), 1067–1080 (2007)
3. Z Farid, R Nordin, M Ismail, Recent advances in wireless indoor localization techniques and system. *J. Comput. Netw. Commun.* **2013**(185138), 1–12 (2013)
4. K Yu, I Sharp, YJ Guo, *Ground-based wireless positioning*, 1st edn. (Wiley, West Sussex, United Kingdom, 2009)
5. Y Zhao, K Liu, Y Ma, Z Li, An improved k-NN algorithm for localization in multipath environments. *EURASIP J. Wireless Commun. Netw.* **2014**(208), 1–10 (2014)
6. MB Zeytinci, V Sari, FK Harmanci, E Anarim, M Akar, Location estimation using RSS measurements with unknown path loss exponents. *EURASIP J. Wireless Commun. Netw.* **2013**(178), 1–14 (2013)
7. P Bahl, VN Padmanabhan, in *IEEE INFOCOM. RADAR: an in-building RF-based user location and tracking system* (The Institute of Electrical and Electronics Engineers, Inc, New York, NY, USA, 2000), pp. 775–784
8. M Youssef, A Agrawala, in *Proceedings of the 3rd International Conference on Mobile Systems, Applications, and Services*. The Horus WLAN location determination system (Association for Computing Machinery, New York, NY, USA, 2005), pp. 205–218
9. K Wu, J Xiao, Y Yi, D Chen, X Luo, LM Ni, CSI-based indoor localization. *IEEE Trans. Parallel Distributed Syst.* **24**(7), 1300–1309 (2013)

10. D Halperin, W Hu, A Sheth, D Wetherall, Tool release: gathering 802.11n traces with channel state information. *ACM SIGCOMM Comput. Commun. Rev.* **41**(1), 53 (2011)
11. TM Schmidl, DC Cox, Robust frequency and timing synchronization for OFDM. *IEEE Trans. Commun.* **45**(12), 1613–1621 (1997)
12. TK Sarkar, O Pereira, Using the matrix pencil method to estimate the parameters of a sum of complex exponentials. *IEEE Antennas Propag. Mag.* **37**(1), 48–55 (1995)
13. N Yilmazer, S Ari, TK Sarkar, Multiple snapshot direct data domain approach and ESPRIT method for direction of arrival estimation. *Digital Signal Process* **18**, 561–567 (2008)
14. GH Golub, CF Van Loan, *Matrix computations*, 4th edn. (Johns Hopkins University Press, Baltimore, MD, USA, 2013)
15. SM Kay, *Fundamentals of statistical signal processing: estimation theory*. (Prentice Hall, New Jersey, USA, 1993), p. 47
16. Y Shen, MZ Win, Fundamental limits of wideband localization: part I: a general framework. *IEEE Trans. Inform. Theory.* **56**(10), 4956–4980 (2010)
17. V Erceg, et al. IEEE P802.11 Wireless LANs: TGn channel models. IEEE document 802.11-03/940r4. (The Institute of Electrical and Electronics Engineers, Inc, New York, NY, USA, 2004)
18. J Medbo, P Schramm. Channel Models for HIPERLAN/2 in Different Indoor Scenarios. ETSI/BRAN document no. 3ERI085B. (European Telecommunications Standards Institute, Valbonne, FRANCE, 1998)
19. Z Sahinoglu, S Gezici, in *IEEE Wireless and Microwave Technology Conference*. Ranging in the IEEE 802.15.4a standard (The Institute of Electrical and Electronics Engineers, Inc., New York, NY, USA, 2006)
20. M Losada, L Zamora-Cadenas, U Alvarado, I Velez, in *IEEE International Conference on Ultra-Wideband*. Performance of an IEEE 802.15.4a ranging system in multipath indoor environments (The Institute of Electrical and Electronics Engineers, Inc., New York, NY, USA, 2011), pp. 455–459

Submit your manuscript to a SpringerOpen<sup>®</sup> journal and benefit from:

- Convenient online submission
- Rigorous peer review
- Immediate publication on acceptance
- Open access: articles freely available online
- High visibility within the field
- Retaining the copyright to your article

---

Submit your next manuscript at ► [springeropen.com](http://springeropen.com)

---